Barrier Effects of Hyperosmolar Signaling in Microvascular Endothelium of Rat Lung

Regine Ragette, Chenzhong Fu, and Jahar Bhattacharya
Department of Medicine, St. Luke's-Roosevelt Hospital Center, College of Physicians and Surgeons, Columbia University, New York 10019

Abstract

We determined the effects of hyperosmolarity on lung microvascular barrier properties by means of the split-drop technique in single venular capillaries of the isolated, blood-perfused rat lung. Using isosmolar and hyperosmolar test solutions (colloid osmotic pressure = 21 cm H_2O), we quantified transcapillary flux at a fixed absorptive capillary pressure, and the capillary hydraulic conductivity (Lp). Loss of barrier function was indicated in flux reversal from isosmolar absorption to hyperosmolar filtration ($P < 0.01$), and by hyperosmolarity-induced Lp increase ($P < 0.01$). Barrier recovery after a 1-min hyperosmolar exposure was delayed > 25 min. The flux reversal was blocked by the tyrosine kinase inhibitors genistein and MDC ($P < 0.01$). Genistein also inhibited the Lp increase ($P < 0.01$). Immunoblots of hyperosmolarity-exposed, cultured rat lung microvascular endothelial cells (RLMEC) and of endothelial cells freshly harvested from lungs given hyperosmolar infusions indicated a genistein-inhibitable enhancement of protein tyrosine phosphorylation. Immunoprecipitation studies indicated tyrosine phosphorylation of the mitogen activated protein kinases (MAPK) ERK1 and ERK2 and the adaptor protein Shc in lysates of RLMEC exposed to hyperosmolar conditions. We conclude that in lung venular capillaries hyperosmolarity deteriorates barrier properties, possibly by inducing tyrosine phosphorylation of endothelial proteins. (*J. Clin. Invest.* 1997. 100:685–692.) Key words: capillary permeability • tyrosine kinase • MAPK • mercuric chloride • lung

Introduction

Hyperpermeability of the lung microvascular barrier, a major cause of pulmonary edema, is determined by endothelial mechanisms which are activated in lung microvascular injury. Although these mechanisms are usually attributed to receptor-mediated endothelial signal transduction, nonreceptor mechanisms may also be important, such as those attributable to microvascular hyperosmolarity. Although hyperosmolarity has been shown to cause endothelial shrinkage in vitro (1) and to increase permeability in some microvascular beds (2–4), the effects of hyperosmolarity on lung microvascular barrier properties remain undetermined.

Barrier deteriorating effects of hyperosmolarity are likely to involve barrier determinants such as interendothelial junctional width and endothelial anchorage to the perimicrovascular matrix. Endothelial shrinkage under hyperosmolar conditions may destabilize barrier properties by increasing junctional width and possibly weakening cell–matrix interactions. In addition, hyperosmolarity induces tyrosine phosphorylation of the p38 mitogen activated protein kinase (MAPK)[1] in murine macrophages (5). Hence, endothelial protein tyrosine phosphorylation which we have shown recently to be a significant receptor-mediated mechanism for increasing lung capillary permeability (6) may also subserve hyperosmolarity-induced barrier deterioration.

In this study, we tested the mechanisms of hyperosmolar barrier regulation in our single vessel model of lung transcapillary liquid exchange (7). Using the split-drop technique, this model allows assessment of permeability in intact vessels, but avoids hemodynamic effects which complicate interpretation of microvascular permeability in traditional whole organ approaches (8). In the split-drop procedure, low capillary pressure (Pc) induces capillary influx (absorption) for test solutions at physiological colloid osmotic pressure (COP) (9). Absorptive flux which is driven by a lumen-directed COP gradient reflects competence of the microvascular barrier because it signifies the ability of the barrier to sustain such a gradient. Barrier competence is also determined by the quantification of the capillary hydraulic conductivity (Lp) which is a measure of the capillary permeability to bulk flow (7). Here, we report experiments in which dextran made hyperosmolar by addition of sucrose caused concentration-dependent loss of barrier function as indicated in a flux reversal from absorption to filtration at identical Pc, and by increase of Lp. This loss of barrier function was blocked by tyrosine kinase inhibitors. These results, together with immunoblotting experiments in lung microvascular endothelial cells, suggest for the first time that hyperosmolar barrier deterioration results from induction of endothelial protein tyrosine phosphorylation.

Methods

Lung preparation. The isolated, blood-perfused rat lung (Sprague-Dawley; Harlan Sprague-Dawley, Inc., Indianapolis, IN) was set up

Address correspondence to Jahar Bhattacharya, M.D., D. Phil., Lung Vascular Biology Laboratory, Columbia University, St. Luke's-Roosevelt Hospital Center, 1000 Tenth Avenue, New York, NY 10019. Phone: 212-523-7310; FAX: 212-523-8005.

Received for publication 5 December 1996 and accepted in revised form 24 April 1997.

J. Clin. Invest.

0021-9738/97/08/0685/08 $2.00
Volume 100, Number 3, August 1997, 685–692
http://www.jci.org

1. *Abbreviations used in this paper:* COP, colloid osmotic pressure; Jv, liquid flux per unit of surface area; Lp, capillary hydraulic conductivity; MAPK, mitogen activated protein kinase(s); Pc, capillary pressure; Pzf, zero filtration pressure; RLMEC, rat lung microvascular endothelial cells.

according to standard procedures (7, 9). Briefly, lungs of anaesthetized rats (450–600 g; 2% halothane inhalation followed by sodium pentobarbital 40 mg/kg, intraperitoneal) were pump-perfused (10–12 ml/min) with autologous rat blood through cannulas inserted in the pulmonary artery and left atrium. A tracheal cannula was used for lung inflation with compressed air. A heat exchanger (model 44TD; Yellow Springs Instruments Co., Yellow Springs, OH) maintained perfusate temperature at 37°C. Recordings of pressures in the pulmonary artery, the left atrium, and the airway (model P23 ID pressure transducer; Gould Statham, Oxnard, CA) were displayed on a multichannel recorder (Gould 2800S; Gould Statham). Zero reference for all pressures was established at the uppermost surface of the lung. Left atrial pressure was maintained at 3 cm H_2O throughout. Airway pressure was held constant at 5 cm H_2O during micropuncture but was cyclically varied to induce ventilation during nonmicropuncture intervals. To prevent drying, the lung surface was covered in plastic wrap. The area of micropuncture was layered with warmed (37°C) silicone oil which was replaced every 5–10 min.

Solutions and reagents for lung experiments. Reagents were obtained from Sigma Chemical Co. (St. Louis, MO), except where specified. All experimental solutions were prepared in isosmolar Ringer's lactate, containing (mM) 144 (Na^+), 1.5 (Ca^{2+}), 123 (Cl^-), 28 (lactate). pH was adjusted to 7.4 (pH Meter; Beckman Instruments, Irvine, CA) and osmolarity to 295 mosM (model 3MO; Advanced Instruments, Inc., Needham Heights, MA) using NaCl. COP was adjusted to 21 cm H_2O (membrane osmometer, model 4100; Wescor Inc., Logan, UT), by adding 4% dextran (70 kD). This was the control solution for determinations of baseline flux under isosmolar conditions and was the vehicle for all test solutes and reagents. Hyperosmolar solutions were prepared by adding sucrose or urea to the control solution. Genistein (4′,5,7-trihydroxyisoflavone) and MDC (GIBCO-BRL, Life Technologies, Gaithersburg, MD), a stable analogue of erbstatin, were prepared as stock solutions in dimethylsulfoxide. GRGDSP peptide (Peninsula Laboratories Inc., Belmont, CA) was prepared in 0.9% NaCl.

Transcapillary flux measurement by the split-drop procedure. Our split-drop procedure has been described several times (7, 9). Briefly, lungs were positioned on a vibration-free air table (Micro-G; Technical Manufacturing Corp., Peabody, MA) for stereomicroscopy (×150, model SZH; Olympus, Tokyo, Japan), and videorecording (camera, Panasonic WV-CD5; monitor, Panasonic WV-5410; videorecorder, Panasonic AG-6050; Matsushita Communication Industrial Co., Yokohama, Japan). Venules of 15–35 μm in diameter were identified by their convergent flow patterns (9). As required for the split-drop procedure, micropipettes (tip diameter ~ 5 μm) were pulled (Sachs-Fleming Puller, model P-84; Sutter Instrument Co., Novato, CA) and bevelled (beveller; Sutter Instrument Co.) from siliconized glass tubing (1 mm diameter; Glass Co. of America, Bargaintown, NJ). They were filled with either research grade castor oil (Sigma Chemical Co.) stained with Sudan black or with experimental solution.

Pulmonary blood flow was stopped to equalize vascular pressures. Pc was determined as the left atrial pressure under stopped flow conditions. By use of successive micropunctures, an oil drop was first injected into the experimental venule and then split with the experimental solution. Micropuncture sites were sealed with further oil injections, then micropipettes were removed. Changes in split-length (distance between margins of the split oil drop) in the first minute were videorecorded, then quantified on-screen by microcaliper (resolution 1 μm; Mitutoyo Corp., Tokyo, Japan), in a frame-by-frame replay. The oil–endothelial contact does not deteriorate the endothelial barrier within the < 2 min duration of the split-drop procedure (9), after which blood flow is reinstated. Split-drop data were rejected in the event of blood leaks into the split-drop or out of the capillary.

Split length, hence split-drop volume, increases with liquid entry into the capillary (absorption), but decreases with liquid efflux (filtration). Microvessel diameter remains constant. Liquid flux per unit of surface area (Jv) at time 0, is estimated according to our previously reported analysis (7, 9). Briefly, split length and capillary diameter measurements determined by microcaliper (Mitsutoyo Corp.) from a frame-by-frame video replay (×400; resolution 1 μm) are applied to the cylinder formula to calculate split-drop volume and surface area. Jv is calculated at different Pc by differentiating at time 0, the slope of the exponential regression of split-drop volume versus time in the first 20–30 s using five or more points. The linear Jv–Pc relation obtained through Jv determinations at two or more Pc, gives Lp as the slope and zero filtration pressure (Pzf) as the x-intercept (further considered in Discussion).

Immunoblotting. Our methods for culturing endothelial cells and immunoblotting endothelial cell lysates for determination of protein tyrosine phosphorylation have been described (10). Fresh rat lung microvascular endothelial cells (RLMEC) were obtained as a generous gift from Dr. Una Ryan (T Cell Sciences, Inc., Boston, MA). The cells were maintained in DME (GIBCO-BRL) supplemented with 10% FBS (Gemini Bio-Products, Calabasas, CA), 10,000 U/ml penicillin, and 10,000 μg/ml streptomycin (Gemini Bio-Products). Cell phenotype was confirmed by positive immunofluorescence staining for Factor VIII antigen (monoclonal mouse anti–human antibodies; Chemicon International, Inc., Temecula, CA) followed by FITC-labeled goat anti–mouse IgG (Sigma Chemical Co.).

For experiments, cells were plated in 12-well dishes (~ 10^4 cells/well) and grown to confluence (3–4 d). Wells were incubated at 37°C with the different experimental solutions. Cells were lysed at 4°C (lysis buffer: [mM] NaCl 150, Tris base 50, EDTA 2 [Bio-Rad Laboratories, Richmond, CA], NaF 50, SDS 0.1%, NP-40 1% [Pierce, Rockford, IL]), scraped, and centrifuged. The supernatants were subjected to 10% SDS-PAGE. After electrophoretic transfer to nitrocellulose, tyrosine phosphorylated proteins were detected using biotinylated antiphosphotyrosine antibodies (ICN Biomedicals, Inc., Irvine, CA) followed by streptavidin–horseradish peroxidase (Jackson ImmunoResearch Labs., West Grove, PA). Immunoblots were developed using enhanced chemiluminescence (DuPont; NEN Research Products, Boston, MA).

Immunoprecipitation. After 10 min of exposure to 295, 350, or 450 mosM (plain or sucrose-enriched Hanks' buffered solution), RLMEC monolayers (~ 10^6 cells/well) were lysed, and the cell lysates incubated overnight with protein A/B beads preadsorbed with anti-ERK1/ERK2 (polyclonal anti–rabbit; Santa Cruz Biotechnology, Santa Cruz, CA) or anti-Shc (monoclonal anti–mouse, Santa Cruz Biotechnology) antibodies. The immunprecipitated proteins were then separated on 10% SDS-PAGE, immunoblotted with respective polyclonal IgG antibodies (Santa Cruz Biotechnology) or biotinylated antiphosphotyrosine antibodies followed by streptavidin–horseradish peroxidase, and developed using enhanced chemiluminescence.

Harvesting fresh lung endothelial cells. We adapted reported magnetic cell-separation procedures (11) to harvest fresh endothelial cells from rat lung homogenates. Separation procedures were performed at 4°C. The rats (Sprague-Dawley, 500 g) were halothane anesthetized and killed with an overdose of pentobarbital (100 mg intraperitoneally). The lungs were inflated through a tracheal cannula, at airway pressure of 5 cm H_2O. Through midline thoracotomy, the pulmonary arteries and left ventricles were cannulated. The experimental condition was established by infusing the lungs with isosmolar or hyperosmolar (450 mosM) dextran for 1 min at 37°C (infusion rate, 10 ml/min; perfusion pressure, 10 cm H_2O). Immediately afterwards, cell responses were inhibited by infusing chilled trypsin (4°C, 0.25% trypsin; Sigma Chemical Co.) until the effluent was cleared of blood.

The peripheral microvessel-rich portions of the lungs were excised. The tissue was diced, immersed in trypsin for 12 h, then homogenized, pelleted (5,000 rpm, 5 min), and resuspended several times using 10% BSA Sigma Chemical Co.) or 5% bovine calf serum (Gemini Bioproducts) in calcium-free buffer solution (0.5% BSA in PBS with 5 mM EDTA). The suspensions were filtered (40 μm pore filter, SQ40S; Pall Biomedical, Inc., Fajardo, Puerto Rico), and centrifuged (1,800 rpm, 15 min) on Ficoll (Pharmacia Biotech, Uppsala, Sweden) to collect the middle, cell-rich layer which was then reclari-

fied by repeated pelleting and resuspension in calcium-free wash buffer.

The final suspensions were incubated overnight with monoclonal mouse anti–human Factor VIII antibody (1:50; Chemicon). Then the samples were pelleted, resuspended in wash buffer to remove excess antibody, and treated with paramagnetic microbeads coated with monoclonal rat anti–mouse IgG (MACS CD4 Multisort Microbeads; Miltenyi Biotech, Gladbach, Germany). After 20 min, the samples were fractionated in a column (MACS Separation Column CS; Miltenyi Biotech) held in a magnet (VarioMACS, Miltenyi Biotech). The effluent containing nonspecific cells was rejected and the column-retained endothelial cell–rich fractions were collected. Endothelial cells were identified by Factor VIII staining and uptake of fluorescent diI-acetyl-LDL (gift from Dr. J. Khoury, Columbia University, NY). By these criteria we established that endothelial cells comprised > 99% of the total cells. Counts by hematocytometer indicated recovery of $> 10^5$ cells/lung. For immunoblotting procedures, cells were pelleted and lysed in 50 μl lysis buffer and processed as described for cultured endothelial cells.

Data analysis. Data are from 190 capillaries in 49 rats. n = number of Jv or Lp as indicated. Group data are presented as mean±SD. Paired differences were tested by the paired t test, and differences among > 2 groups by the ANOVA-Neuman Keul's test. Significance was accepted at $P < 0.05$.

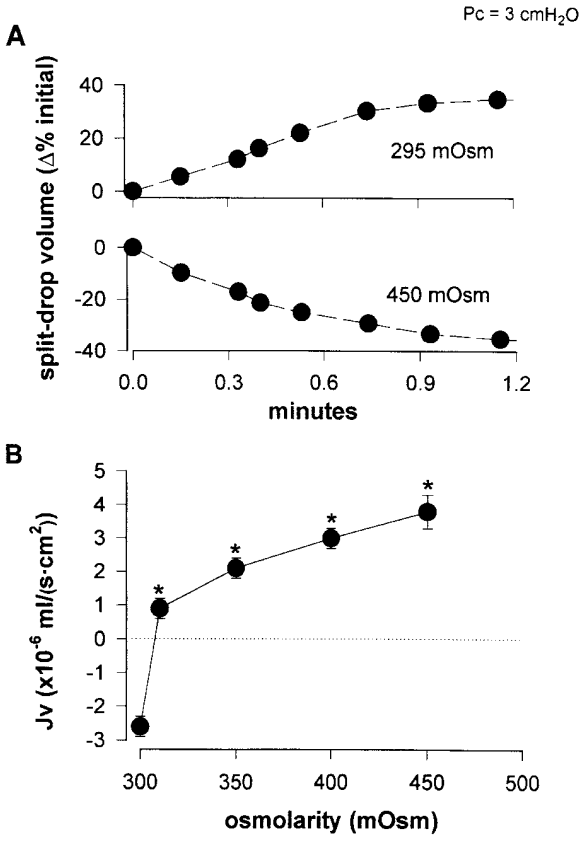

Figure 1. Effect of hyperosmolarity on Jv in single microvessels of rat lung. A single experiment (*A*) shows that split-drop volume increases under isosmolar conditions (absorption) and decreases under hyperosmolar conditions (efflux). Determinations of Jv (*B*) show nonlinear increase with increasing osmolarity. Jv, mean±SD, $n = 4$ for each point; negative Jv indicates absorption, positive Jv efflux. *Significantly different from isosmolar control ($P < 0.1$).

Results

Jv responses to hyperosmolar dextran. Fig. 1 shows split-drop volume changes in single experiments, at Pc = 3 cm H_2O and COP = 21 cm H_2O. Absorptive flux attributable to isosmolar dextran was shown by a 35% increase of split-drop volume in the first min (Fig. 1 *A*, *top*). By contrast, under similar conditions hyperosmolar dextran caused efflux as indicated by the decrease of split-drop volume (Fig. 1 *A*, *bottom*). The isosmolar influx was consistent with normal barrier properties, but the hyperosmolar efflux suggested deteriorated barrier function.

On average, Jv were $-2.6\pm0.5 \times 10^{-6}$ ml/(cm²·s) ($P < 0.01$; $n = 10$) for isosmolar dextran, where the negative sign indicates influx, but were significantly higher at $4.0\pm0.7 \times 10^{-6}$ ml/(cm²·s) ($n = 12$; $P < 0.01$) for hyperosmolar dextran (450 mosM). Efflux increased with increase of hyperosmolarity and was detectable with osmolar increase of as little as 10 mosM above control (Fig. 1 *B*, second data point from left). Because hyperosmolar solutions were prepared by the addition of sucrose to dextran, we ruled out a sucrose-specific effect by determining that urea-enriched hyperosmolar dextran (460 mosM) also caused efflux (Jv = $3.4\pm0.8 \times 10^{-6}$ ml/(cm²·s); $n = 4$).

Since the above efflux responses were obtained during an ~ 1-min capillary exposure to hyperosmolar dextran, in separate experiments we quantified the time to recovery of absorptive flux. Single capillaries were microinfused with hyperosmolar dextran (450 mosM) for 1 min, then reperfused with blood to establish isosmolar conditions. Jv was determined at different time intervals using isosmolar dextran as test solution. Fig.

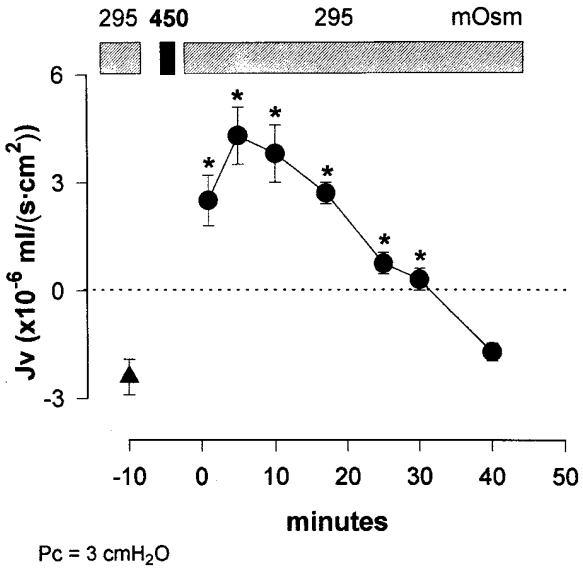

Figure 2. Jv responses to brief hyperosmolar exposure in single microvessels of rat lung. The control group (*triangle*) was infused for 1 min with isosmolar dextran. The test group (*circles*) was microinfused for 1 min with dextran of 450 mosM, then reperfused with isosmolar blood. Jv responses were determined by the split-drop technique using isosmolar dextran as test solution. Note that hyperosmolar infusion caused efflux (positive Jv) which persisted > 25 min. Jv, mean±SD, $n = 4$ for each point. *Significantly different from isosmolar control ($P < 0.5$).

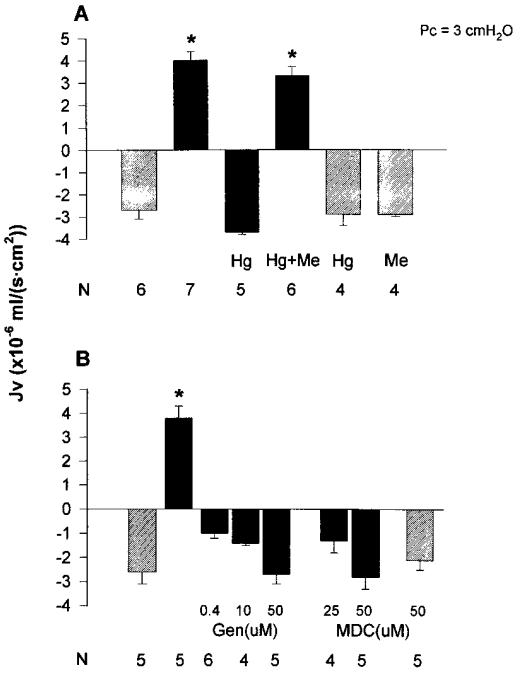

Figure 3. Inhibition of hyperosmolarity-induced efflux in single microvessels of rat lung. Jv responses (mean±SD, $n = 4$ for each group) were determined in the presence of AQP1 inhibitor, $HgCl_2$ (*A*), and after 30 min of preinfusion with tyrosine kinase inhibitors genistein and MDC (*B*). Isosmolar conditions (295 mosM, *light bars*) caused absorption (negative Jv), whereas hyperosmolar conditions (450 mosM, *dark bars*) caused efflux (positive Jv). 3 mM $HgCl_2$ given with hyperosmolar dextran blocked efflux (*A*, *Hg*). This effect was reversed by 6 mM mercaptoethanol (*A*, *Hg + Me*). $HgCl_2$ (*A*, *Hg*) and mercaptoethanol (*A*, *Me*) did not affect isosmolar absorption. Note that genistein and MDC caused concentration-dependent inhibition of hyperosmolar efflux (*B*, *Gen* and *MDC*). MDC did not affect isosmolar influx (*B*, *MDC*). *Significantly different from isosmolar control ($P < 0.1$).

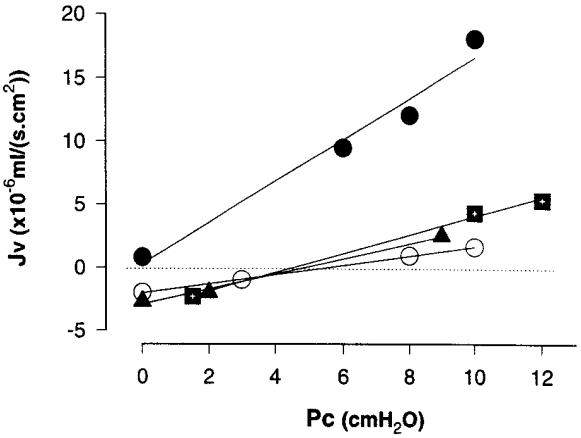

Figure 4. Plots of split drop flux (*Jv*) against capillary pressure (*Pc*) from single venular capillaries of rat lung single experiments. Lines drawn by linear regression ($P < 0.05$). Lp determined from slope. The zero-filtration pressure, Pzf, is given by the Pc at Jv = 0. Note hyperosmolarity increases Lp and decreases Pzf as compared with isosmolar control (295 mosM, *unfilled circles*). Both effects are abolished by $HgCl_2$ and genistein. 450 mosM, *filled circles*; 450 mosmM + $HgCl_2$, *filled squares*; 450 mosM + genistein, *filled triangles*.

2 shows that despite return to the isosmolar condition, efflux increased further for 5 min and took as long as 40 min to return to baseline. These findings indicate that brief hyperosmolar exposure caused prolonged loss of endothelial barrier function despite restoraton of isosmolar conditions.

Inhibition of hyperosmolar efflux

Mercurial inhibition (Fig. 3 A). $HgCl_2$ (3 mM) given with isosmolar dextran caused no difference in absorptive flux as compared with control. However, given with hyperosmolar dextran (450 mosM), $HgCl_2$ caused absorptive flux, which indicated that the usual efflux response to hyperosmolarity was inhibited by mercuric chloride. This inhibition was reversed by mercaptoethanol (6 mM), as previously reported (12). Given alone, mercaptoethanol did not affect influx under control conditions, therefore it did not cause barrier injury.

Tyrosine kinase inhibition (Fig. 3 B). The prolonged barrier recovery to hyperosmolar exposure indicated the involvement of barrier deteriorating signal transduction mechanisms. We have shown recently that the tyrosine kinase inhibitors, genistein and MDC, block receptor-mediated increases of lung microvascular permeability (6). These inhibitors have different modes of action: genistein inhibits ATP binding to tyrosine kinase, while MDC inhibits by competing for the kinase substrate (13). Capillary preinfusions for 30 min with genistein or MDC caused concentration-dependent inhibitions of hyperosmolar efflux, but had no effect on control absorption rates. These results implicated tyrosine kinase activation in the hyperosmolar efflux response.

Effect of GRGDSP. We considered that integrins which establish cell–matrix interactions may induce barrier effects by transducing hyperosmolar cell shape changes (14, 15). However GRGDSP (1.7 mM), a synthetic peptide which blocks integrin–ligand interaction by binding to the integrin RGD-recognition sequence (15), failed to inhibit the hyperosmolar (450 mosM) efflux (Jv = 4.4±0.5, $n = 5$). Therefore, our findings do not implicate integrins in the present responses.

Lp and Pzf responses to hyperosmolarity

Since the flux reversal from influx to efflux at constant Pc suggested deterioration of the capillary barrier, we directly determined Lp to quantify barrier function. Single experiments are shown in Fig. 4 and the group data are shown in Table I. Hyperosmolar dextran (450 mosM) increased Lp three times above isosmolar control and markedly decreased Pzf. Given

Table I. Effect of Hyperosmolarity on Barrier Properties of Venular Capillaries in Rat Lung

Test solution	No.	Lp	Pzf
mosM		*($\times 10^{-7}$ ml/s·cm²·cm H_2O)*	*(cm H_2O)*
295	5	4.9±0.9	6.0±1.0
450	5	16.0±0.8*	0.2±0.8*
450 + $HgCl_2$	4	6.8±0.4‡	4.3±0.4‡
450 + genistein	4	6.0±0.5	4.9±0.8

*$P < 0.01$ compared with 1st row. ‡$P < 0.01$ compared with 2nd row. $HgCl_2$, 3 mM; genistein, 100 mM.

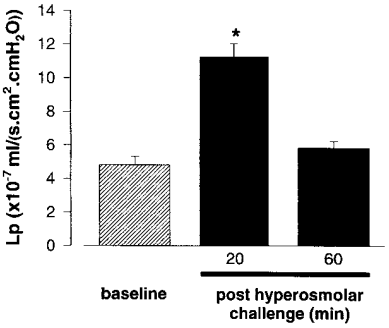

Figure 5. Hydraulic conductivity (*Lp*) of venular capillaries in rat lung, after brief hyperosmolar challenge. Baseline, control data before hyperosmolar challenge. After hyperosmolar challenge, microvessels were infused for 1 min with hyperosmolar dextran, then reperfused with isosmolar blood. All Lp (mean±SD, $n = 3$ for each group) determined using isosmolar test solution. *Different from baseline at $P < 0.05$.

separately, genistein and $HgCl_2$ almost completely inhibited both effects.

To determine Lp recovery after a brief hyperosmolar challenge, we used a protocol similar to that of the flux recovery experiments (Fig. 2). We gave a single 1-min microvascular infusion of hyperosmolar dextran. Then, after reestablishing blood flow to reinstate isosmolar conditions, we determined Lp using isosmolar test solution. Fig. 5 shows that, similar to the flux reversal data, Lp remained significantly elevated 20 min after return to isosmolar conditions. At this time, the Pzf was 0.6±0.4 cm H_2O, which was markedly lower than the baseline Pzf, which for this group averaged 5.5±0.5 cm H_2O ($P < 0.05$, $n = 3$). By 60 min, barrier recovery was evident in that neither Lp nor Pzf differed significantly from baseline.

Hyperosmolarity enhances protein tyrosine phosphorylation in RLMEC

To determine endothelial signaling mechanisms, we considered that, similar to murine macrophages (5), hyperosmolarity may induce protein tyrosine phosphorylation in endothelial cells. Hence, we exposed RLMEC to hyperosmolar medium, then immunoblotted the cell lysates for phosphotyrosine (see Methods). A 5-min hyperosmolar exposure caused concentration-dependent enhancement of tyrosine phosphorylation of several endothelial proteins (Fig. 6 *A*). Enhancement of tyrosine phosphorylation was most consistent for bands corresponding to proteins of 28–32, 42–46, and 50 kD. Only occasional and weak enhancement of a band at 38 kD was evident.

The phosphorylation was maximally enhanced at 400 mosM (Fig. 6 *A*, lane *3*). Comparison of lanes *4* and *5* in Fig. 6 *A* indicates that similar levels of hyperosmolarity obtained by addition of sucrose and urea, respectively, caused similar enhancements of protein tyrosine phosphorylation. This result reaffirmed that the endothelial effects of hyperosmolarity were not sucrose specific. Preincubations of RLMEC with genistein blocked hyperosmolarity-induced enhancement of tyrosine phosphorylation on all bands (Fig. 6 *A*, lane *6*).

Hyperosmolarity-induced tyrosine phosphorylation was markedly inhibited by preincubation with $HgCl_2$ (Fig. 6 *A*, lane *7*). To test whether this inhibition was attributable to nonspecific effects, we determined the mercurial effect on tyrosine phosphorylation induced by a nonosmolar mechanism. Accordingly, Fig. 6 *B* shows that $HgCl_2$ also blocked receptor-mediated tyrosine phosphorylation induced by vitronectin (10). We conclude, therefore, that mercurial inhibition of protein tyrosine phosphorylation was irrelevant to the inducing stimulus.

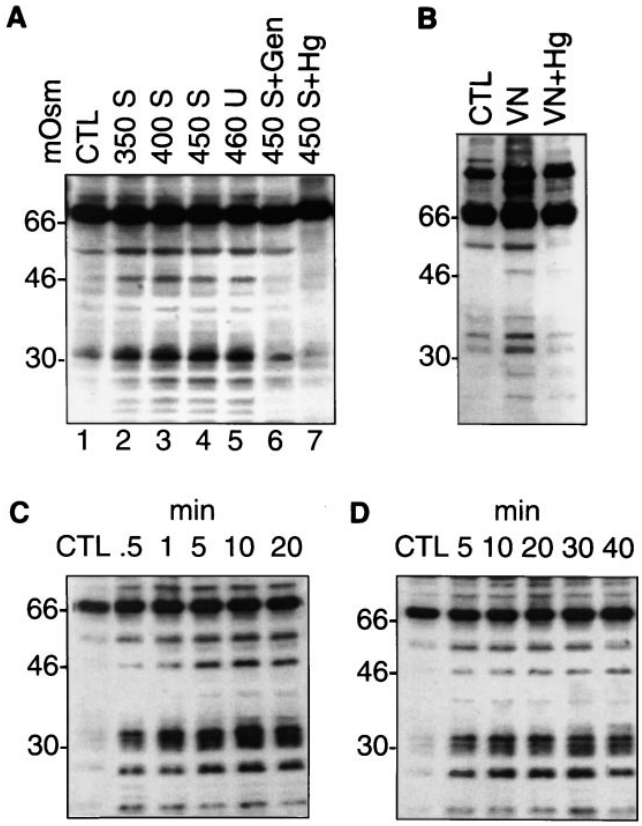

Figure 6. Effect of hyperosmolarity on protein tyrosine phosphorylation in RLMEC. RLMEC were incubated at 37°C for 5 min in medium which was isosmolar (295 mosM; *CTL*) or made hyperosmolar by addition of sucrose (*S*) or urea (*U*). Cells were lysed, subjected to SDS-PAGE, and immunoblotted with antiphosphotyrosine antibody. Increasing osmolarity increased protein tyrosine phosphorylation (*A*, lanes *1–4*), which was blocked by preincubation with 100 μM genistein (*A*, lane *5*) or coexposure to 3 mM $HgCl_2$ (*A*, lane *6*). Cell incubations (*B*) with 400 ml/ml vitronectin (*VN*) caused increased tyrosine phosphorylation, which was also blocked by coexposure to 3 mM $HgCl_2$ (*VN + Hg*). Cells incubated with medium of 450 mosM for increasing intervals (*C*) showed time-dependent enhancement of protein tyrosine phosphorylation. Cells exposed for 5 min to medium of 450 mosM followed by incubation with control medium of 295 mosM for increasing intervals show persistence of protein tyrosine phosphorylation despite restoration of isosmolar conditions (*D*). Molecular weight markers appear on the left.

Continuous exposure of endothelial monolayers to hypertonic medium (450 mosM) progressively enhanced protein tyrosine phosphorylation which peaked at 10 min (Fig. 6 *C*). A 5-min hyperosmolar (450 mosM) exposure followed by replacement with isosmolar medium resulted in enhanced phosphorylation that was sustained for 40 min (Fig. 6 *D*). Thus, similar to the data for sustained barrier deterioration (Figs. 2 and 5), enhanced protein tyrosine phosphorylation was sustained despite restoration of isosmolar conditions.

Immunoprecipitates of control and hyperosmolarity-treated cells using anti-ERK1 (44 kD), anti-ERK2 (42 kD), and anti-Shc (46, 52, 56, and 66 kD) antibodies followed by SDS-PAGE and immunoblotting procedures with respective antibodies re-

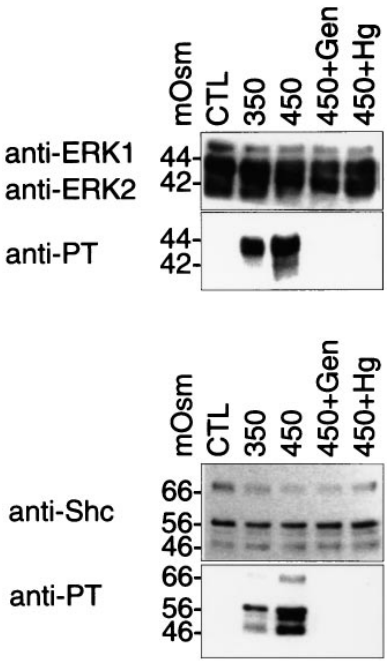

Figure 7. Immunoprecipitation and immunoblotting of ERK 1, ERK 2, and Shc in RLMEC. Confluent RLMEC were incubated at 37°C for 10 min with isosmolar (295 mosM, *CTL*) or hyperosmolar (350 and 450 mosM) medium. Cells were lysed and immunoprecipitated with respective antibodies followed by SDS-PAGE and immunoblotting using indicated antibodies. Note that in antiphosphotyrosine (*anti-PT*) immunoblots, tyrosine phosphorylation increases with increasing osmolarity. Tyrosine phosphorylation was inhibited by 100 μM genistein (*Gen*) and 3 mM $HgCl_2$ (*Hg*). Molecular weight markers appear on the left.

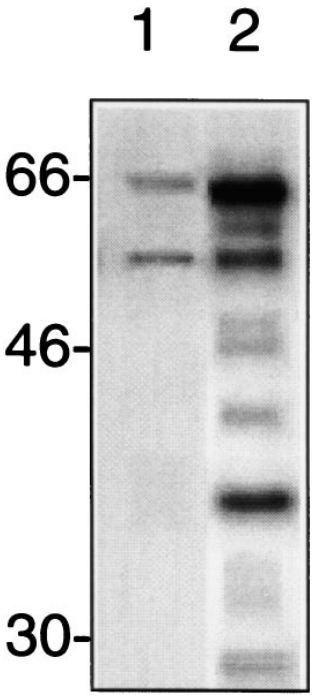

Figure 8. Protein tyrosine phosphorylation in native RLMEC. Microvascular endothelial cells were isolated from rat lungs infused at 37°C for 1 min with isosmolar (295 mosM, lane *1*) or hyperosmolar (450 mosM, lane *2*) dextran. Cells were lysed, subjected to SDS-PAGE, and immunoblotted with antiphosphotyrosine antibody. Molecular weight markers appear on the left.

vealed single bands for ERK1 and ERK2 (Fig. 7, *top*) and four bands for Shc, corresponding to the four Shc subunits (Fig. 7, *bottom*). These results indicated equal protein expression in control and hyperosmolarity-treated cells. Antiphosphotyrosine immunoblotting showed marked tyrosine phosphorylation on ERK1, ERK2, and Shc in cells exposed to hyperosmolar solutions. The tyrosine phosphorylation was concentration-dependent and was completely abolished by genistein and $HgCl_2$. No tyrosine phosphorylation was present under isosmolar conditions.

Since cultured and native endothelial cells may respond differently to osmolar stress, we determined the profile of endothelial protein tyrosine phosphorylation in native microvascular endothelial cells recovered as described (see Methods). From lungs given 1-min infusions of either 295 or 450 mosM dextran (COP = 21 cm H_2O) endothelial cells were harvested, lysed, and immunoblotted with antiphosphotyrosine. The result of one experiment is shown in Fig. 8. Cells from hyperosmolarity-treated lungs showed a pattern of enhanced protein tyrosine phosphorylation which was similar to RLMEC, except that phosphorylation of the band at 38 kD was considerably more pronounced.

Discussion

In one set of experiments, we exposed single lung capillaries to either isosmolar or hyperosmolar dextran, then determined flux direction across the capillary barrier under conditions that favor absorption in a capillary with normal barrier properties. Although in the control experiments isosmolar dextran caused the expected absorption, under identical conditions hyperosmolar dextran caused efflux. This flux reversal suggested barrier deterioration. Hence, in a second set of experiments, we directly quantified hyperosmolarity-induced barrier deterioration as a threefold Lp increase. The important finding was that the flux reversal and the Lp increase both were inhibited by tyrosine kinase inhibitors, suggesting that the effects were attributable to tyrosine kinase activation. We determined that these inhibitors had no individual nonspecific effects on barrier properties, because neither caused flux reversal when given alone with isosmolar dextran. Tyrosine kinase activation was also indicated in the immunoblotting evidence for protein tyrosine phosphorylation which was obtained in lysates both of cultured lung endothelial cells directly exposed to hyperosmolar solutions, and of endothelial cells freshly harvested from lungs given hyperosmolar infusion. Immunoblots showed marked enhancement of protein tyrosine phosphorylation on proteins of 28–32, 42–46, and 50–66 kD. By immunoprecipitation we identified these proteins to be the MAP kinases ERK1, ERK2, and the adaptor protein Shc. Therefore, we confirmed that hyperosmolar stress deteriorates capillary barrier properties (2–4), and we showed for the first time that the barrier deteriorating effects may involve endothelial signaling through protein tyrosine phosphorylation.

The hyperosmolarity-induced reduction of Pzf occurred not only within the first minute, but, together with the Lp increase, was sustained for > 20 min. Pzf is defined by the quantity $[Pi + \sigma(\pi c - \pi i)]$ where Pi is interstitial pressure, σ is the osmotic reflection coefficient, πc and πi are, respectively, the plasma and the interstitial COP (8). Because of the small sucrose reflection coefficient ($\sigma < 0.04$; reference 16), it is unlikely that sucrose itself contributed significantly to the net force gradient. Based on our previous data (17), we may assume $Pi = 0$. Hence, the decrease of Pzf was attributable either to a decrease of σ or an increase of πi. We cannot distinguish between these possibilities from these data.

Cell shrinkage. Hyperosmolar stress rapidly decreases endothelial volume (18), hence our hypertonic protocols proba-

bly caused shrinkage of capillary endothelial cells. As proposed by others (1, 2), endothelial shrinkage attributable to endothelial water loss may have widened interendothelial junctions and thereby increased permeability. We tested the shrinkage hypothesis by exposing capillaries briefly to hyperosmolar conditions and then reestablishing baseline isosmolarity. These protocols are expected to cause cell volume changes with a time constant in seconds because of the high water permeability of the endothelial cell membrane. If hyperosmolarity-induced capillary hyperpermeability were solely shrinkage dependent, restoration of isosmolarity should rapidly reverse shrinkage and concomitantly correct the hyperpermeability. By contrast, permeability increased in the first 5 min after restoration of isosmolar conditions, and remained elevated for $>$ 20 min (Figs. 2 and 6). This prolonged persistence of hyperpermeability under isosmolar conditions argues against endothelial shrinkage as the direct cause for the barrier deterioration.

A second argument against the shrinkage hypothesis is derived from the experiments with tyrosine kinase inhibitors. We point out that genistein and MDC which were given under hyperosmolar conditions are not water channel inhibitors and are unlikely to have blocked endothelial shrinkage. However, both blocked the flux reversal and genistein inhibited the Lp increase. Hence, we conclude that the increase of microvascular permeability did not result directly from cell shrinkage. In the next section we consider the possibility that hyperosmolarity-induced endothelial shrinkage initiated protein tyrosine phosphorylation as a signal for endothelial barrier deterioration.

Protein tyrosine phosphorylation. The hyperosmolarity-induced barrier deterioration and enhancement of endothelial protein tyrosine phosphorylation were similar in several respects. First, both effects were rapidly detectable. Thus, enhancement of endothelial phosphorylation was well developed within 1 min of hyperosmolar exposure either to cultured monolayers (Fig. 6 *C*) or to the lung vascular bed (Fig. 8). Second, both effects were blocked by the tyrosine kinase blockers. Third, both effects showed concentration dependence. Thus, increasing osmolarity increased flux reversal and intensity of phosphorylation. Fourth, both effects were sustained beyond the period of hyperosmolar exposure. Thus, a brief hyperosmolar challenge induced sustained barrier deterioration (Figs. 2 and 5) and enhanced phosphorylation (Fig. 6 *D*). These similarities suggest that the hyperosmolar barrier and the phosphorylation responses are causally related.

Hyperosmolar exposure progressively increased protein tyrosine phosphorylation in RLMEC over a 10-min period (Fig. 6 *C*). However, since barrier quantification was not obtained for hyperosmolar exposures of $>$ 1 min, it remains unclear whether the increasing phosphorylation corresponded to further barrier deterioration. Interestingly, in the period after the 1-min hyperosmolar challenge, the enhanced phosphorylation persisted for up to 40 min (Fig. 6 *D*) although barrier properties progressively recovered to baseline (Figs. 2 and 5). It is possible that barrier deteriorating processes are initiated by the tyrosine phosphorylation, but that barrier protective processes subsequently activated oppose the initial effects and progressively restore barrier function.

The data in Fig. 8 are the first phosphotyrosine immunoblotting data for cells harvested from experimentally treated lungs. Since protein phosphorylation responses may differ between cultured and in situ endothelial cells, we used this new approach to determine in situ endothelial phosphorylation in hyperosmolar lungs. By the present separation methods, endothelial cells were recovered in sufficient numbers ($> 10^5$/lung) and purity from microvessel-enriched lung regions for immunoblotting studies. The studies revealed marked enhancement of protein tyrosine phosphorylation in cells recovered from hyperosmolarity-exposed lungs in a pattern similar to that of cultured RLMEC exposed to hyperosmolar stress. However, phosphorylation on the band at 38 kD was more pronounced in freshly recovered cells. Cultured endothelial cells grow as flat monolayers of cuboidal cells and may be phenotypically modified in vitro, whereas native endothelial cells are elongated and arrange longitudinally along the capillary lumen (19). These phenotypic and geometrical differences could induce different responses between the cell types.

The causal link between enhanced tyrosine phosphorylation and capillary hyperpermeability was suggested in the genistein experiments, in that genistein inhibited both effects. We conclude that endothelial protein phosphorylation may be critical to the hyperosmolarity-induced increase of capillary permeability. We reported recently that ligation and aggregation of the lung endothelial $\alpha v\beta 3$ integrin causes a genistein-inhibitable increase of lung capillary permeability and enhancement of lung endothelial protein tyrosine phosphorylation (6, 10). The similarity of the present data suggests that interventions as disparate as integrin ligation and hyperosmolarity converge on protein tyrosine phosphorylation as the common signaling pathway for endothelial barrier deterioration.

Although the mechanisms are not clear, it is possible that the mechanical effects of endothelial cell shrinkage initiated enhanced protein tyrosine phosphorylation. Cell membrane deformations attributable to cell water loss may be transduced by the activation of tyrosine kinases such as those of the c-src family. These are potentially implicated here because the hyperpermeability was inhibited by MDC, a synthetic erbstatin analogue which specifically inhibits src-family kinases (13). Evidently, the mechanical stimulus arising from osmolar stress is sensitively graded by the responding element in the cell, because both hyperpermeability (Fig. 1) and enhanced protein tyrosine phosphorylation (Fig. 6 *A*) increased in a concentration-dependent manner with increasing osmolarity. Our present findings, together with previous studies of shear stress (20, 21) and mechanical stretch (22), suggest that protein tyrosine phosphorylation serves as an important step in cell signaling induced by mechanosensitive stimuli. We rule out integrin–extracellular matrix interactions in these responses, because the hyperosmolarity-induced hyperpermeability was insensitive to integrin inhibition by an RGD-containing peptide.

Although $HgCl_2$ blocked the hyperosmolar permeability increase, we must emphasize that because of potential mercurial toxicity this result provides the least certain indication of barrier deteriorating mechanisms in our data. We used the agent because previous reports implicated $HgCl_2$ in inhibition of lung liquid transport across transmembrane water channels (12, 23). However, because it alkylates sulfhydryl groups, $HgCl_2$ is likely to induce nonspecific effects. For example, here we show that $HgCl_2$ is also a potent tyrosine kinase inhibitor. It blocked not only hyperosmolarity- but also vitronectin-induced protein tyrosine phosphorylation (10). Hence, the ability of $HgCl_2$ to inhibit lung flux responses must be interpreted with caution because the inhibition may be attributable to nonspecific toxic effects.

Our findings are relevant to the emerging understanding that environmental stresses such as hyperosmolar exposure induce a variety of cell signaling responses (24–29). Previously, the p38 kinase, a member of the MAPK family, was shown to be tyrosine phosphorylated in murine macrophages and pre-B lymphocytes exposed to hyperosmolar solutions (5). Here we show that the MAP kinases ERK1 and ERK2 are tyrosine phosphorylated in endothelial cells exposed to hyperosmolarity. Although we did not immunoprecipitate the p38 kinase, a strong band at 38 kD in freshly harvested endothelial cells suggests that the p38 kinase may also have been tyrosine phosphorylated. Although these data indicate involvement of the MAPK pathway, the role of MAPK in these barrier responses remains unknown.

Hyperpermeability of the endothelial barrier is associated with cytoskeletal events such as actin polymerization (30). Although the signaling pathways are unclear, we speculate that c-src may be activated because this hyperosmolarity-induced efflux was inhibited by MDC, a specific c-src inhibitor (13). Moreover, the c-src substrate, Shc, was tyrosine phosphorylated under hyperosmolar conditions. Since Shc binds F-actin (31), it is possible that under hyperosmolar conditions c-src activation may tyrosine phosphorylate Shc and thereby activate cytoskeletal proteins to promote endothelial barrier deterioration.

Finally, we point out that our findings must be interpreted with caution since they were obtained in our specific experimental model, namely the single venular capillary of the isolated, blood-perfused lung. Our findings indicate that hyperosmolar solutions increase permeability of venular capillaries, possibly by inducing well defined endothelial signaling responses such as protein tyrosine phosphorylation. Although these responses suggest the existence of a novel mechanism for induction of lung endothelial hyperpermeability, the extent to which such mechanisms are applicable to the physiologically perfused, intact lung under clinical hyperosmolar conditions requires further investigation.

Acknowledgments

Ms. Rashmi Patel assisted with cell culture, cell separation, and other procedures.

The work was supported by National Institutes of Health grants HL-53625 and HL-36024 and by a fellowship award to Regine Ragette from the Stony Wold-Herbert Fund, Inc.

References

1. Shepard, J.M., S.K. Goderie, N. Brzyski, P.J. Del Vecchio, A.B. Malik, and H.K. Kimelberg. 1987. Effects of alterations in endothelial cell volume on transendothelial albumin permeability. *J. Cell. Physiol.* 133:389–394.

2. Rapoport, S.I., W.R. Ohno, and K.D. Pettigrew. 1980. Quantitative aspects of reversible osmotic opening of the blood brain barrier. *Am. J. Physiol. 238 (Regulatory Integrative Comp. Physiol. 7)*:R421–R431.

3. Granger, D.N., J.P. Granger, R.A. Brace, R.E. Parker, and A.E. Taylor. 1978. Analysis of the permeability characteristics of the cat intestinal capillaries. *Circ. Res.* 44:335–344.

4. Rasio, E.A., M. Bendayan, and C.A. Goresky. 1981. The effect of hyperosmolarity on the permeability and structure of the capillaries of the isolated rete mirabilae of the eel. *Circ. Res.* 49:661–676.

5. Han, J., J.D. Lee, L. Bibbs, and R.J. Ulevitch. 1994. A MAP kinase targeted by endotoxin and hyperosmolarity in mammalian cells. *Science (Wash. DC)*. 265:808–811.

6. Tsukada, H., X. Ying, C. Fu, S. Ishikawa, P. McKweon-Longo, S. Albelda, S. Bhattacharya, B.A. Bray, and J. Bhattacharya. 1995. Ligation of endothelial avb3 integrin increases capillary hydraulic conductivity of rat lung. *Circ. Res.* 77:651–659.

7. Bhattacharya, J. 1988. Hydraulic conductivity of lung venules determined by split-drop technique. *J. Appl. Physiol.* 64:2562–2567.

8. Parker, J.C., M.A. Perry, and A.E. Taylor. 1984. Permeability of microvascular barrier. *In* Edema. N.C. Staub and A.E. Taylor, editors. Raven Press, New York. 143 pp.

9. Qiao, R.L., and J. Bhattacharya. 1991. Segmental barrier properties of the pulmonary microvascular bed. *J. Appl. Physiol.* 71:2152–2159.

10. Bhattacharya, S., C. Fu, J. Bhattacharya, and S. Greenberg. 1995. Soluble ligands of the avb3 integrin mediate enhanced tyrosine phosphorylation of multiple proteins in adherent bovine pulmonary artery endothelial cells. *J. Biol. Chem.* 270:16781–16787.

11. Miltenyi, S., W. Müller, W. Weichel, and A. Radbruch. 1990. High gradient magnetic cell separation with MACS. *Cytometry.* 11:231–238.

12. Folkesson, H.G., M.A. Matthay, H. Hasegawa, F. Kheradmand, and A.S. Verkman. 1994. Transcellular water transport in lung alveolar epithelium through mercury-sensitive water channels. *Proc. Natl. Acad. Sci. USA.* 91:4970–4974.

13. Miyamoto, S., H. Teramoto, O.A. Coso, J.S. Gutkind, P.D. Burbelo, S.K. Akiyama, and K.M. Yamada. 1995. Integrin function. Molecular hierarchies of cytoskeletal and signaling molecules. *J. Cell. Biol.* 131:791–805.

14. Ingber, D. 1991. Integrins as mechanochemical transducers. *Curr. Opin. Cell. Biol.* 3:841–848.

15. Wilson, E., S. Krishnankutty, and H.E. Ives. 1995. Mechanical strain of rat vascular smooth muscle cells is sensed by specific extracellular matrix/integrin interactions. *J. Clin. Invest.* 96:2364–2372.

16. Taylor, A.E., and K.A. Gaar. 1970. Estimation of equivalent pore radii of pulmonary capillaries and alveolar membranes. *Am. J. Physiol.* 218:1133–1140.

17. Bhattacharya, J., M.A. Gropper, and N.C. Staub. 1984. Interstitial fluid pressure gradient measured by micropuncture in excised dog lung. *J. Appl. Physiol.* 56:271–277.

18. O'Neill, W.C., and J.D. Klein. 1992. Regulation of vascular endothelial cell volume by Na-K-2Cl cotransport. *Am. J. Physiol. 262 (Cell Physiol. 31)*: C436–C444.

19. McDonald, D.M. 1994. Endothelial gaps and permeability of venules in rat tracheas exposed to inflammatory stimuli. *Am. J. Physiol. 266 (Lung Cellular and Molecular Physiol. 10)*: L61–L83.

20. Ayajiki, K., M. Kindermann, M. Hecker, I. Fleming, and R. Busse. 1996. Intracellular pH and tyrosine phosphorylation but not calcium determine shear stress–induced nitric oxide production in native endothelial cells. *Circ. Res.* 78: 750–758.

21. Oda, A., K. Yokoyama, M. Murata, M. Tokuhira, K. Nakamura, M. Handa, K. Watanabe, and Y. Ikeda. 1995. Protein tyrosine phosphorylation in human platelets during shear stress–induced platelet aggregation (SIPA) is regulated by glycoprotein (GP) Ib/IX as well as GP IIb/IIIa and requires intact cytoskeleton and endogenous ADP. *Thromb. Haemostasis.* 74:736–742.

22. Yano, Y., J. Geibel, and B.E. Sumpio. 1996. Tyrosine phosphorylation of pp125FAK and paxillin in aortic endothelial cells induced by mechanical strain. *Am. J. Physiol. 271 (Cell Physiol. 40)*:C635–C649.

23. Schnitzer, J.E., and O.H. Phil. 1996. Aquaporin-1 in plasma membrane and caveolae provides mercury-sensitive water channels across lung endothelium. *Am. J. Physiol. 270 (Heart Circ. Physiol. 39)*:H416–H422.

24. Klein, J.D., and W.C. O'Neill. 1995. Volume-sensitive myosin phosphorylation in vascular endothelial cells: correlation with Na-K-2Cl cotransport. *Am. J. Physiol. 269 (Cell Physiol. 38)*:C1524–C1531.

25. Santell, L., R.L. Rubin, and E.G. Levin. 1993. Enhanced phosphorylation and dephosphorylation of a histone-like protein in response to hyperosmotic and hypoosmotic conditions. *J. Biol. Chem.* 268:21443–21447.

26. Oyama, K. 1996. cGMP accumulation induced by hypertonic stress in *Dictyostelium discoideum. J. Biol. Chem.* 271:5574–5579.

27. Brewster, J.L., T. De Valoir, N.D. Dwyer, E. Winter, and M.C. Gustin. 1993. An osmosensing signal transduction pathway in yeast. *Science (Wash. DC)*. 259:1760–1763.

28. Schüller, C., J.L. Brewster, M.R. Alexander, M.C. Gustin, and H. Ruis. 1994. The HOG pathway controls osmotic regulation of transcription via the stress response element (STRE) of the *Saccharomyces cerevisiae* CTT1 gene. *EMBO (Eur. Mol. Biol. Org.) J.* 13:4382–4389.

29. Tokishita, S., and T. Mizuno.1994. Transmembrane signal transduction by the *Escherichia coli* osmotic sensor, EnvZ: intermolecular complementation of transmembrane signal transduction. *Mol. Microbiol.* 13:435–444.

30. Suttorp, N., M. Polley, J. Seybold, H. Schnittler, W. Seeger, F. Grimminger, and K. Aktories. 1995. Adenosine diphosphate-ribosylation of G-Actin by botulinum C2 toxin increases endothelial permeability in vitro. *J. Clin. Invest.* 87:1575–1584.

31. Thomas, D., S.D. Patterson, and R.A. Bradshaw. 1995. Scr homologous and collagen (Shc) protein binds to F-actin and translocates to the cytoskeleton upon nerve growth factor stimulation in PC12 cells. *J. Biol. Chem.* 270:28924–28931.